Supplementary Material

Public mouse liver transcriptomics datasets

The hepatic ChREBP overexpression data in C57BL/6J mice were extracted from (GSE61576, (1)) and the data on hepatocyte-specific *Hnf-4*α knockout mice and wildtype controls were extracted from (GSE10390, (2)).

Construction and production of shRNAs using self-complementary AAV vectors

To construct the self-complementary AAV (scAAV) 2/8-U6-ChREBP, the scAAV2-LP1-hFIXco backbone vector (3) was restricted with BamHI and BbsI and the 3493 bp fragment was isolated and ligated. Restriction with BamHI removed hFIXco and partially deleted the LP1 promoter. The U6 promoter driving the expression of the construct was cloned into the vector in antisense orientation. shRNA construct directed against ChREBP and scramble construct were ordered as oligonucleotides (shRNA; 5'-aat tcA AAA AAT GTA GTT TGA AGA TGT GGG TCT CGA GAC CCA CAT CTT CAA ACT ACA TC-3' and 3'-ggc caG ATG TAG TTT GAA GAT GTG GGT CTC GAG ACC CAC ATC TTC AAA CTA CAT TTT TT-5', scramble; 5'-aat tcG TTG TAA GTG GAG GTT TAA GTC TCG AGA CTT AAA CCT CCA CTT ACA ACA CCG GT-3' and 3'-ggc caA CCG GTG TTG TAA GTG GAG GTT TAA GTC TCG AGA CTT AAA CCT CCA CTT ACA AC-5'), denatured at 99 °C for 10 min and annealed by cooling down to RT. The duplex oligonucleotides were cloned into the vector using EcoRI and AgeI. Production, purification and titration of the AAV2/8 viruses encoding the shRNA directed against ChREBP (AAV-ChREBP) and the scrambled control (AAV-Scramble) were performed as described (4, 5).

Hepatic lipid and acylcarnitine profiles

Frozen liver was homogenized in ice-cold PBS. Hepatic lipid contents were assessed using commercial available kits (Roche Diagnostics, Basel, Switzerland) after lipid extraction (6). Hepatic fatty acid and acylcarnitine profiles were analyzed as previously described (7, 8).

Hepatic metabolome analysis

Freeze-dried liver (2 mg) was collected in a 2 mL tube followed by the addition of 1 mL ice-cold methanol:water (1:1) containing the following internal standards: D_3-aspartic acid, D_3-serine, D_5-glutamine, D_3-glutamate, $^{13}C_3$-pyruvate, $^{13}C_6$-isoleucine, $^{13}C_6$-glucose, $^{13}C_6$-fructose-1,6-biphosphate, $^{13}C_6$-G6P, adenosine-$^{15}N_5$-monophosphate and guanosine-$^{15}N_5$-monophosphate (5 µM). For the extraction of metabolites 1 mL of chloroform was added and the samples were needle sonicated (8 watt, 40 joule). The homogenate was centrifuged for 5 min at 14,000 rpm at 4 degrees Celsius. The “polar” top layer was transferred to a new 1.5 mL tube and dried in a vacuum concentrator. Dried samples were dissolved in 100 µL methanol/water (6/4; v/v). The metabolomic analysis was performed as described previously (9, 10). Interpretation of the data was performed in the Xcalibur software (Thermo scientific). Statistical analysis of the acquired data were done in an R environment using the *ggplot2, ropls* and *mixOmics* packages (11-13).

Glycolytic enzyme capacities (V_{max})

Liver tissue was homogenized in ice-old PBS containing Phosphatase Inhibitor Cocktail 2 & 3 (1:100; P5726 P0044, Sigma-Aldrich) and Protease Inhibitor Cocktail (1:25, 11697498001, Sigma-Aldrich), centrifuged for 10 minutes at 600xg, after which the supernatant was collected. V_{max} assays on these lysates were carried out using NAD(P)H-linked assays at 37 degrees Celsius in a Synergy H4 plate reader (BioTek™) using different (0, 2x, 4x and 8x) dilutions. The reported V_{max} values represent total capacity of all isoenzymes in the cell at saturating concentrations of all substrates and expressed per extracted cell protein. Four different dilutions of extract were used to check for linearity. In nearly all cases at least 2 dilutions were proportional to each other and these were used for further calculation. All enzymes were expressed as µmoles of substrate converted per minute per mg of extracted protein. Protein determination was carried out using the Bicinchoninic Acid kit (BCA™ Protein Assay kit, Pierce). Based on the cytosolic concentrations described

in literature, we have designed an assay medium that was as close as possible to the *in vivo* situation, whilst at the same time experimentally feasible. The standardized *in vivo*-like assay medium contained 150 mM potassium (14-17), 5 mM phosphate (14, 18), 15 mM sodium (14, 19), 155 mM chloride (20, 21), 0.5 mM calcium, 0.5 mM free magnesium (14, 22, 23) and 0.5-10.5 mM sulfate. For the addition of magnesium, it was taken into account that ATP and ADP bind magnesium with a high affinity. The amount of magnesium added equalled the concentration of either ATP or ADP plus 0.5 mM, such that the free magnesium concentration was 0.5 mM. Since the sulfate salt of magnesium was used the sulfate concentration in the final assay medium varied in a range between 0.5 and 10.5 mM. The assay medium was buffered at a pH of 7.0 (24-29) by using a final concentration of 100 mM TRIS-HCl (pH 7.0). To this end an assay mixture containing 100 mM Tris-HCl (pH 7.0), 15 mM NaCl, 0.5 mM $CaCl_2$, 140 mM KCl, and 0.5-10.5 mM $MgS0_4$ was prepared. In addition to the assay medium, the concentrations of the coupling enzymes, allosteric activators and substrates for each enzyme were as follows: Phosphoglucose isomerase (GPI; EC 5.3.1.9) – 0.4 mM $NADP^+$, 1.8 U/mL G6P dehydrogenase (EC 1.1.1.49), and 2 mM fructose 6-phosphate as start reagent. Aldolase (ALD; EC 4.1.2.13) – 0.15 mM NADH, 0.6 U/mL glycerol-3P-dehydrogenase (EC 1.1.1.8), 1.8 U/mL triosephosphate isomerase (EC 5.3.1.1), and 2 mM fructose 1,6-bisphosphate as start reagent. Glyceraldehyde-3-phosphate dehydrogenase (GAPDH; EC 1.2.1.12) – 0.15 mM NADH, 1 mM ATP, 24 U/mL 3-phosphoglycerate kinase (EC 2.7.2.3), and 5 mM 3-phosphoglyceric acid as start reagent. Enolase (ENO; EC 4.2.1.11) – 0.15 mM NADH, 1 mM ADP, 50 U/ml pyruvate kinase (EC 2.7.1.40), 15 U/mL L-lactate dehydrogenase (EC 1.1.1.27), and 1 mM 2-phosphoglyceric acid as start reagent. Pyruvate kinase (PK) – 0.15 mM NADH, 1 mM ADP, 1 mM fructose 1,6-bisphosphate, 60 U/mL L-lactate dehydrogenase (EC 1.1.1.27) and 2 mM phosphoenolpyruvate as start reagent.

Quantification of acetyl-CoA precursor pool enrichments, *de novo* lipogenesis, fatty acid elongation and cholesterol synthesis

Mice received sodium 1-^{13}C-acetate (99 atom %, Isotec/Sigma- Aldrich, St. Louis, MO, USA) via the drinking water (2%) during the 48 hours prior to sacrifice. Hepatic lipids were hydrolyzed and derivatized as described (30). The fatty acid and cholesterol-mass isotopomer distributions were determined by gas chromatography mass spectrometry (GCMS) and used in mass isotopomer distribution analysis algorithms to calculate acetyl-CoA precursor pool enrichments, *de novo* fractional fatty acid and cholesterol synthesis rates, as well as the fraction of oleate and stearate generated by chain elongation of pre-existing palmitate (30). Absolute fatty acid and cholesterol synthesis were calculated from the fractional synthesis rates and hepatic fatty acid and cholesterol contents, and expressed per liver. The amount of 'old fat' was calculated by deducting the amount of fatty acids synthesized by *de novo* lipogenesis and chain elongation from the total amount of hepatic fatty acids.

Gene expression analysis

Total RNA from liver was isolated using TRI-Reagent (Sigma-Aldrich Corp.). For qPCR, cDNA was obtained by reverse transcription and amplified using primers and probes listed in Table S1. mRNA levels were calculated based on a calibration curve, expressed relative to the expression of 36b4 (Taqman) or rpl32 (SYBR green) and normalized to expression levels in L-*G6pc*$^{+/+}$ shScramble-treated mice. For RNA sequencing, initial quality check and RNA quantification of the samples was performed by capillary electrophoresis using the LabChip GX (Perkin Elmer). Non-degraded RNA-samples were used for subsequent sequencing analysis. Sequence libraries were generated using the 3'QuantSeq sample preparation kits (LeXogen). The obtained cDNA fragment libraries were sequenced on an Illumina HiSeq2500 using default parameters (single read 1x50bp) in pools of multiple samples. The fastQ files where aligned to build Mus_musculus GRCm38 Ensemble Release 82 reference genome using HISAT (31) with default settings. Before gene quantification

SAMtools was used to sort the aligned reads (32). The gene level quantification was performed by HTSeq-count (33). The extracted raw count file (ENSG, counts) was analyzed in the MADMAX (34). After transformation (log_2CPM), normalization (Voom) (35) was performed to generate the differentially expressed genes. Table S2A contains the normalized RNA-seq data presented in heatmaps. Additional RNA-seq data can be made available upon reasonable request to the corresponding author.

Targeted proteomics

Targeted proteomics was used to quantify G6PC, ChREBP, APOB, MTTP and TM6SF2 in homogenized liver tissue using isotopically labeled peptide standards (GLGVDLLWTLEK for G6PC, LGFDTLHGLVSTLSAQPSLK for ChREBP, VQGVEFSHR for APOB, ATSVTTYK and SDSSIILQER for MTTP, and TPFTYR for TM6SF2), containing ^{13}C-labeled lysine/arginine (PolyQuant GmbH, Bad Abbach, Germany) as described previously (36). The following alterations were made: lipids were extracted from the liver homogenates with diethyl ether prior to the proteomics workflow and the concentrations were related to the total peptide content, which was determined by a colorimetric peptide assay after tryptic digestion and SPE cleanup (Thermo Scientific). The concentrations of endogenous peptides were calculated from the known concentration of the standard and expressed in fmol/µg of total peptide and expressed relative to the values in the control group.

***In silico* predictions**

In order to identify potential ChREBP and HNF-4α binding sites in the TM6SF2 gene a combination of computational analysis was performed and publicly available ChIP-seq datasets were evaluated. Putative HNF-4α (DR-1) sites in the mouse and human gene were derived from (37). Putative ChREBP sites in the mouse and human gene were derived from (38) and (39) respectively.

ChIP-qPCR on the mouse *Tm6sf2* promoter

Livers were homogenized in PBS and cross-linked with 0.5M Di (N-succinimidyl) glutarate (DSG) for 45 min at room temperature. The pellet was resuspended in PBS

and cross-linked with 1% formaldehyde for 15 min at room temperature. 0.125M glycine was added and the samples were incubated 5 min at room temperature. The pellets were homogenized in 500 µL lysis buffer (5 mM Pipes, 85 mM KCL, 1% Nonidet P-40 with protease inhibitors) and incubated on ice for 10 min. Cell pellets were lysed in 300 µL nuclear lysis buffer (50 mM Tris-HCl pH 8.1, 10 mM EDTA, 1% SDS with protease inhibitors) and sonicated at 30% maximum power eight times for 10 seconds. The supernatant was diluted in IP-dilution buffer (0.01% SDS, 1.1% Trition X 100, 1.2 mM EDTA, 16.7 mM Tris-Cl pH 8.1, 167 mM NaCl with protease inhibitors) to a volume of 3 mL. The supernatant was precleared with 50% Protein A agarose/salmon sperm DNA beads (Santa Cruz) 100 µL of the supernatant was removed and used for direct amplification of DNA (input sample). The remaining sample was immunoprecipitated overnight at 4°C with 3 µg ChREBP (Novus), HNF4A (Santa Cruz) or normal rabbit IgG antibody (Santa Cruz). On the following day IPs were precleared with 50% Protein A agarose/salmon sperm DNA beads. Subsequently, the beads were washed in low salt buffer (0.1% SDS, 1% Triton X 100, 2 mM EDTA, 20 mM Tris-HCl pH 8, 150 mM NaCl), high salt buffer (0.1% SDS, 1% Triton X 100, 2 mM EDTA, 20 mM Tris-HCl pH 8, 500 mM NaCl) and LiCl buffer (1% Nonidet P-40, 24.1 mM sodium deoxycholate, 1 mM EDTA, 10 mM Tris-HCl pH 8, 250 mM LiCl). The beads and input were boiled in 10% chelex followed by incubation with 10 µg/mL proteinase K at 55° C for 30 min. DNA was purified using the PCR Clean-up Extraction Kit (Macherey-Nagel), after which qPCR was performed. Primers for ChIP-PCR are listed in Table S1.

Nascent VLDL isolation and -analysis

Chylomicrons were isolated from the fresh final plasma samples using an Optima TM LX tabletop ultracentrifuge (Beckman Instruments Inc., Palo Alto, CA, USA) at 100.000xg for 15 minutes at 10 degrees Celsius (40) and stored separately. Nascent VLDL particles (0.15M NaCl; d<1.006) were isolated from the remaining samples using an Optima TM LX tabletop ultracentrifuge (Beckman Instruments Inc., Palo

Alto, CA, USA) at 625.000xg for 100 minutes at 18 degrees Celsius (41). TG, cholesterol and phospholipid concentrations of nascent VLDLs were determined using commercially available kits (Roche Diagnostics and Wako Chemicals, Neuss, Germany). VLDL particle diameter was estimated using the following formula: diameter (nm) = 60 x ((0.211 x TG/phospholipid in mg/dL) + 0.27)) (24). VLDL particle volume was derived from the calculated diameter using the following formula: particle volume = 4/3 x π x (0,5 x particle diameter)^3. Volumes of nascent VLDL containing equal amounts of TG (125 nmol) were pooled, and lipids were extracted with methanol and cold ether. The remaining VLDL proteins were incubated at 100 degrees Celsius for 5 minutes in loading buffer, subsequently subjected to SDS-PAGE with 15 nmol TG loaded per lane. Apolipoprotein (apo)B was determined using antibodies against anti-mouse apoB raised in rabbit (Biodesign, Saco, ME). Horseradish peroxidase-conjugated anti-rabbit antibodies from donkey (Amersham Pharmacia Bioscience, GE Healthcare) were used as a secondary antibody for all immunoblots. Protein bands were detected using SuperSignal West Pico Chemiluminescent Substrate System (Thermo Fisher Scientific, Rockford, IL, USA). Band densities were determined using a Gel Doc XR system (Biorad, Hercules, CA, USA).

Cell reporter assays

CV1 cells (ATCC) cultured in 48-wells plates in DMEM (Gibco 31966-021) were transiently transfected using FuGENE HD Transfection Reagent (Promega). Human and mouse Tm6sf2 promoter constructs (-1500/+100 bp; Thermo Fisher) were ligated into pGL3-Basic using restriction enzymes XhoI and KpnI. The human or mouse PGL3/Tm6sf2 promoter luciferase reporters (100 ng of each) or empty pGL3-Basic luciferase construct (Promega; 100 ng) were co-transfected with pcDNA3.1/ murine ChREBPα, pcDNA3.1/ murine ChREBPβ, pcDNA3.1/murine MLX (kind gifts from M. Herman, 50 ng of each, for shuttling see (42)), pcDNA3.1/murine HNF-4α (a kind gift from J.W. Jonker, 50 ng), or a combination, and filled up with pcDNA3.1 to

achieve a total amount of 150 ng. After 48 hours cells were lysed and firefly-to-renilla luciferase activities were assessed using a Dual-Luciferase Reporter Assay System (Promega). Within one experiment transfections were performed in triplicate, and experiments were repeated at least three times.

References

1. Benhamed F, Denechaud PD, Lemoine M, Robichon C, Moldes M, Bertrand-Michel J, Ratziu V, et al. The lipogenic transcription factor ChREBP dissociates hepatic steatosis from insulin resistance in mice and humans. J Clin Invest 2012;122:2176-2194.
2. Holloway MG, Miles GD, Dombkowski AA, Waxman DJ. Liver-specific hepatocyte nuclear factor-4alpha deficiency: greater impact on gene expression in male than in female mouse liver. Mol Endocrinol 2008;22:1274-1286.
3. Nathwani AC, Gray JT, McIntosh J, Ng CY, Zhou J, Spence Y, Cochrane M, et al. Safe and efficient transduction of the liver after peripheral vein infusion of self-complementary AAV vector results in stable therapeutic expression of human FIX in nonhuman primates. Blood 2007;109:1414-1421.
4. Hermens WT, ter Brake O, Dijkhuizen PA, Sonnemans MA, Grimm D, Kleinschmidt JA, Verhaagen J. Purification of recombinant adeno-associated virus by iodixanol gradient ultracentrifugation allows rapid and reproducible preparation of vector stocks for gene transfer in the nervous system. Hum Gene Ther 1999;10:1885-1891.
5. Seppen J, Bakker C, de Jong B, Kunne C, van den Oever K, Vandenberghe K, de Waart R, et al. Adeno-associated virus vector serotypes mediate sustained correction of bilirubin UDP glucuronosyltransferase deficiency in rats. Mol Ther 2006;13:1085-1092.
6. Bligh EG, Dyer WJ. A rapid method of total lipid extraction and purification. Can J Biochem Physiol 1959;37:911-917.
7. Muskiet FA, van Doormaal JJ, Martini IA, Wolthers BG, van der Slik W. Capillary gas chromatographic profiling of total long-chain fatty acids and cholesterol in biological materials. J Chromatogr 1983;278:231-244.
8. Derks TG, Boer TS, van Assen A, Bos T, Ruiter J, Waterham HR, Niezen-Koning KE, et al. Neonatal screening for medium-chain acyl-CoA dehydrogenase (MCAD) deficiency in The Netherlands: the importance of enzyme analysis to ascertain true MCAD deficiency. J Inherit Metab Dis 2008;31:88-96.
9. Koenis DS, Medzikovic L, van Loenen PB, van Weeghel M, Huveneers S, Vos M, Evers-van Gogh IJ, et al. Nuclear Receptor Nur77 Limits the Macrophage Inflammatory Response through Transcriptional Reprogramming of Mitochondrial Metabolism. Cell Rep 2018;24:2127-2140 e2127.
10. Baardman J, Verberk SGS, Prange KHM, van Weeghel M, van der Velden S, Ryan DG, Wust RCI, et al. A Defective Pentose Phosphate Pathway Reduces Inflammatory Macrophage Responses during Hypercholesterolemia. Cell Rep 2018;25:2044-2052 e2045.
11. Rohart F, Gautier B, Singh A, Le Cao KA. mixOmics: An R package for 'omics feature selection and multiple data integration. PLoS Comput Biol 2017;13:e1005752.
12. Thevenot EA, Roux A, Xu Y, Ezan E, Junot C. Analysis of the Human Adult Urinary Metabolome Variations with Age, Body Mass Index, and Gender by

Implementing a Comprehensive Workflow for Univariate and OPLS Statistical Analyses. J Proteome Res 2015;14:3322-3335.
13. Wickham H. ggplot2. In: Use R!; 2009.
14. Guynn RW, Veloso D, Lawson JW, Veech RL. The concentration and control of cytoplasmic free inorganic pyrophosphate in rat liver in vivo. Biochem J 1974;140:369-375.
15. Kristensen LO. Associations between transports of alanine and cations across cell membrane in rat hepatocytes. Am J Physiol 1986;251:G575-584.
16. Tschopp J, Schroder K. NLRP3 inflammasome activation: The convergence of multiple signalling pathways on ROS production? Nat Rev Immunol 2010;10:210-215.
17. Rorsman P, Trube G. Glucose dependent K+-channels in pancreatic beta-cells are regulated by intracellular ATP. Pflugers Arch 1985;405:305-309.
18. Conley KE, Blei ML, Richards TL, Kushmerick MJ, Jubrias SA. Activation of glycolysis in human muscle in vivo. Am J Physiol 1997;273:C306-315.
19. Lidofsky SD, Xie MH, Sostman A, Scharschmidt BF, Fitz JG. Vasopressin increases cytosolic sodium concentration in hepatocytes and activates calcium influx through cation-selective channels. J Biol Chem 1993;268:14632-14636.
20. Breitwieser GE, Altamirano AA, Russell JM. Osmotic stimulation of Na(+)-K(+)-Cl- cotransport in squid giant axon is [Cl-]i dependent. Am J Physiol 1990;258:C749-753.
21. Janssen LJ, Sims SM. Acetylcholine activates non-selective cation and chloride conductances in canine and guinea-pig tracheal myocytes. J Physiol 1992;453:197-218.
22. Ingwall JS. Phosphorus nuclear magnetic resonance spectroscopy of cardiac and skeletal muscles. Am J Physiol 1982;242:H729-744.
23. Murphy E, Steenbergen C, Levy LA, Raju B, London RE. Cytosolic free magnesium levels in ischemic rat heart. J Biol Chem 1989;264:5622-5627.
24. Bárány M. Biochemistry of Smooth Muscle Contraction. In: Academic Press; 1996.
25. Bruch P, Schnackerz KD, Gracy RW. Matrix-bound phosphoglucose isomerase. Formation and properties of monomers and hybrids. Eur J Biochem 1976;68:153-158.
26. Civelek VN, Hamilton JA, Tornheim K, Kelly KL, Corkey BE. Intracellular pH in adipocytes: effects of free fatty acid diffusion across the plasma membrane, lipolytic agonists, and insulin. Proc Natl Acad Sci U S A 1996;93:10139-10144.
27. Groen AK, Vervoorn RC, Van der Meer R, Tager JM. Control of gluconeogenesis in rat liver cells. I. Kinetics of the individual enzymes and the effect of glucagon. J Biol Chem 1983;258:14346-14353.
28. Ishibashi H, Cottam GL. Glucagon-stimulated phosphorylation of pyruvate kinase in hepatocytes. J Biol Chem 1978;253:8767-8771.
29. Oudard S, Arvelo F, Miccoli L, Apiou F, Dutrillaux AM, Poisson M, Dutrillaux B, et al. High glycolysis in gliomas despite low hexokinase transcription and activity correlated to chromosome 10 loss. Br J Cancer 1996;74:839-845.
30. Oosterveer MH, van Dijk TH, Tietge UJ, Boer T, Havinga R, Stellaard F, Groen AK, et al. High fat feeding induces hepatic fatty acid elongation in mice. PLoS One 2009;4:e6066.
31. Kim D, Langmead B, Salzberg SL. HISAT: a fast spliced aligner with low memory requirements. Nat Methods 2015;12:357-360.
32. Li H, Handsaker B, Wysoker A, Fennell T, Ruan J, Homer N, Marth G, et al. The Sequence Alignment/Map format and SAMtools. Bioinformatics 2009;25:2078-2079.
33. Anders S, Pyl PT, Huber W. HTSeq--a Python framework to work with high-throughput sequencing data. Bioinformatics 2015;31:166-169.

34. Lin K, Kools H, de Groot PJ, Gavai AK, Basnet RK, Cheng F, Wu J, et al. MADMAX - Management and analysis database for multiple ~omics experiments. J Integr Bioinform 2011;8:160.
35. Law CW, Chen Y, Shi W, Smyth GK. voom: Precision weights unlock linear model analysis tools for RNA-seq read counts. Genome Biol 2014;15:R29.
36. de Boer JF, Schonewille M, Boesjes M, Wolters H, Bloks VW, Bos T, van Dijk TH, et al. Intestinal Farnesoid X Receptor Controls Transintestinal Cholesterol Excretion in Mice. Gastroenterology 2017;152:1126-1138 e1126.
37. Yevshin I, Sharipov R, Kolmykov S, Kondrakhin Y, Kolpakov F. GTRD: a database on gene transcription regulation-2019 update. Nucleic Acids Res 2019;47:D100-D105.
38. Poungvarin N, Chang B, Imamura M, Chen J, Moolsuwan K, Sae-Lee C, Li W, et al. Genome-Wide Analysis of ChREBP Binding Sites on Male Mouse Liver and White Adipose Chromatin. Endocrinology 2015;156:1982-1994.
39. Jeong YS, Kim D, Lee YS, Kim HJ, Han JY, Im SS, Chong HK, et al. Integrated expression profiling and genome-wide analysis of ChREBP targets reveals the dual role for ChREBP in glucose-regulated gene expression. PLoS One 2011;6:e22544.
40. Kendrick JS, Chan L, Higgins JA. Superior role of apolipoprotein B48 over apolipoprotein B100 in chylomicron assembly and fat absorption: an investigation of apobec-1 knock-out and wild-type mice. Biochem J 2001;356:821-827.
41. Pietzsch J, Subat S, Nitzsche S, Leonhardt W, Schentke KU, Hanefeld M. Very fast ultracentrifugation of serum lipoproteins: influence on lipoprotein separation and composition. Biochim Biophys Acta 1995;1254:77-88.
42. Hoogerland JA, Lei Y, Wolters JC, de Boer JF, Bos T, Bleeker A, Mulder NL, et al. Glucose-6-Phosphate Regulates Hepatic Bile Acid Synthesis in Mice. Hepatology 2019;70:2171-2184.

Figure Legends Supporting Figures

Figure S1: Related to Figure 2. (A) Box and-whisker plots presenting concentration and total content of hepatic free cholesterol (FC) and phospholipid (PL) in L-*G6pc*$^{+/+}$ and L-*G6pc*$^{-/-}$ mice treated with either shChREBP or scrambled shRNA (shSCR; n = 7-9). (B) Heatmaps presenting z-score normalized mRNA expression of genes involved in cholesterol biosynthesis in L-*G6pc*$^{+/+}$ and L-*G6pc*$^{-/-}$ mice treated with shChREBP or shSCR (n = 8-9). (C) Box and-whisker plots presenting fractional cholesterol synthesis rates and absolute cholesterol synthesis in L-*G6pc*$^{+/+}$ and L-*G6pc*$^{-/-}$ mice, treated with shChREBP or shSCR (n = 6-8). (D) Heatmaps presenting z-score normalized hepatic mRNA levels of ER stress markers in L-*G6pc*$^{+/+}$ and L-*G6pc*$^{-/-}$ mice treated with shChREBP or shSCR (n = 8-9).

*p < 0.05, **p <0.01 indicates significance compared to shSCR. ^^^p <0.001 indicates significance compared to L-*G6pc*$^{+/+}$ mice. Table S2A contains raw values and statistics for data presented in heatmaps.

Figure S2: Related to Figure 3. (A) *ex vivo* adipocyte lipolysis at different time points and box and-whisker plots presenting lipolysis rate in L-*G6pc*$^{+/+}$ and L-*G6pc*$^{-/-}$ mice treated with either shChREBP or scrambled shRNA (shSCR; n = 7-9). (B) Western Blot of apoB48 protein in nascent VLDL samples of L-*G6pc*$^{+/+}$ and L-*G6pc*$^{-/-}$ mice treated with either shChREBP or shSCR. Equal amounts of TG were loaded onto the gel for all groups (n = 3).

Figure S3: Related to Figure 4. (A) Hepatic gene expression levels in C57BL/6J mice treated with GFP-expressing (Ad-GFP) or ChREBP-expressing (Ad-ChREBP) (n = 4-5, GSE 61576, (24)). (B) Schematic presentation of putative ChREBP (#1-2, dark grey) and HNF-4α (DR-1, light grey) response elements within the human *TM6SF2* promoter. The solid line represents the part of the promoter that was covered by the human reporter gene while the

dashed line represents a region further downstream. (C) Box and-whisker plots presenting firefly-to-renilla luciferase activities for the empty pGL3-Basic reporter after transfection with HNF-4α, MLX, ChREBPα and ChREBPβ plasmids (n = 3 independent experiments, each experiment performed in triplicate). (D) Box and-whisker plots presenting firefly-to-renilla luciferase activities for the human Tm6sf2 gene reporter after transfection with HNF-4α, MLX, ChREBPα and ChREBPβ plasmids (n = 3 independent experiments, each experiment performed in triplicate). (E) Box and-whisker plots presenting hepatic Tm6sf2 mRNA levels in hepatocyte-specific *Hnf-4α* knockout mice (data of 4 pooled knockout samples expressed relative to a pooled wildtype control sample, GSE10390, (49)) and in chow-fed full-body ChREBP null mice (n = 4-5, (50)) in comparison to their respective wildtype controls.

*p < 0.05, **p <0.01, ***p < 0.001 indicates significance compared to Ad-GTP for panel A (at FDR= 5%), compared to pcDNA3.1 for panels C-D, and compared to wildtype for panel E. ^p < 0.05, ^^p < 0.01 indicates significance compared to control for panels C-D. #p < 0.05, ##p < 0.01 indicates significance compared to pcDNA3.1+HNF-4α for panels C-D.

Figure S1

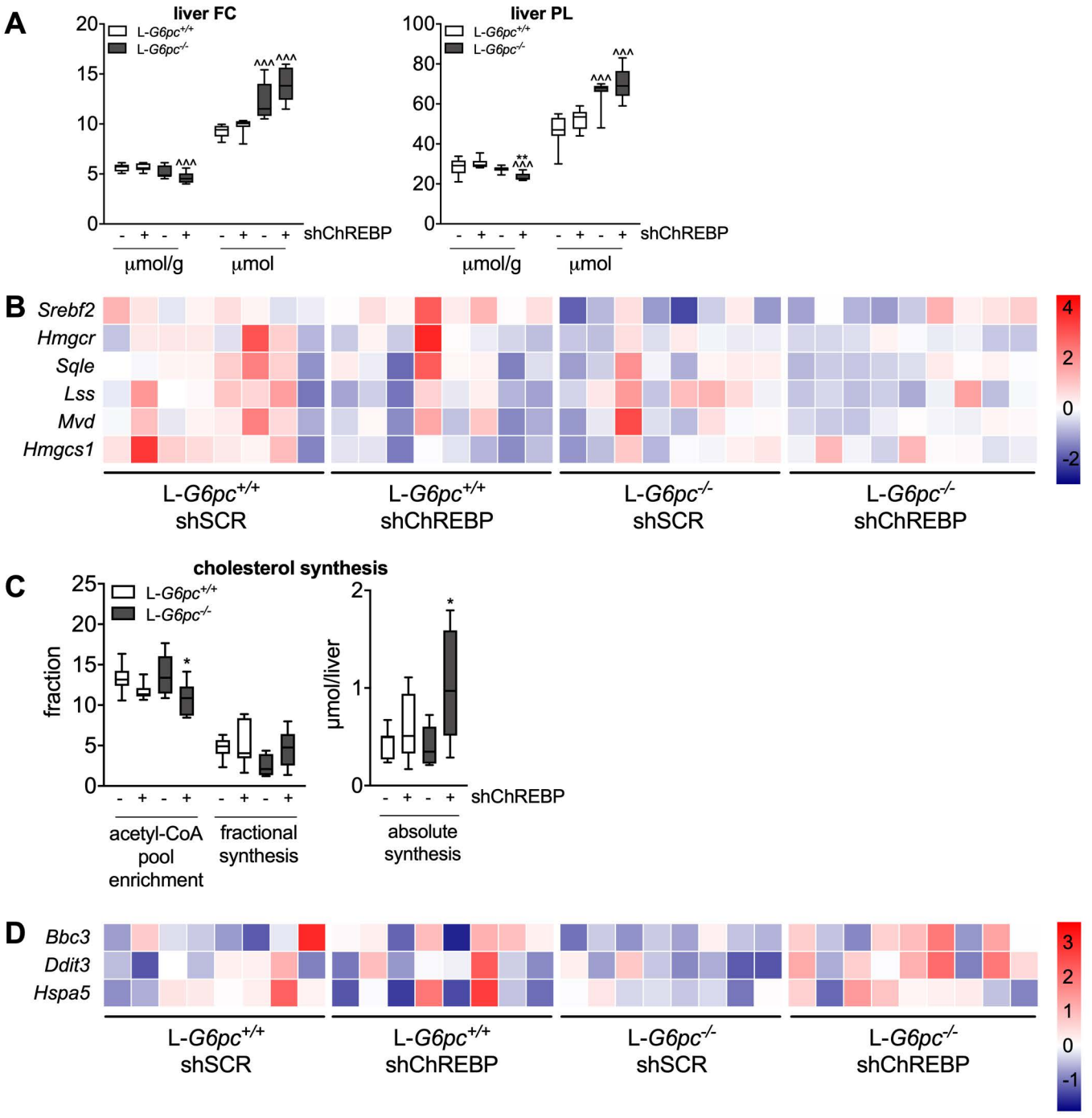
A
liver FC
liver PL
L-G6pc+/+
L-G6pc-/-
shChREBP
µmol/g
µmol
B
Srebf2
Hmgcr
Sqle
Lss
Mvd
Hmgcs1
L-G6pc+/+ shSCR
L-G6pc+/+ shChREBP
L-G6pc-/- shSCR
L-G6pc-/- shChREBP
C
cholesterol synthesis
fraction
µmol/liver
acetyl-CoA pool enrichment
fractional synthesis
absolute synthesis
D
Bbc3
Ddit3
Hspa5

Figure S2

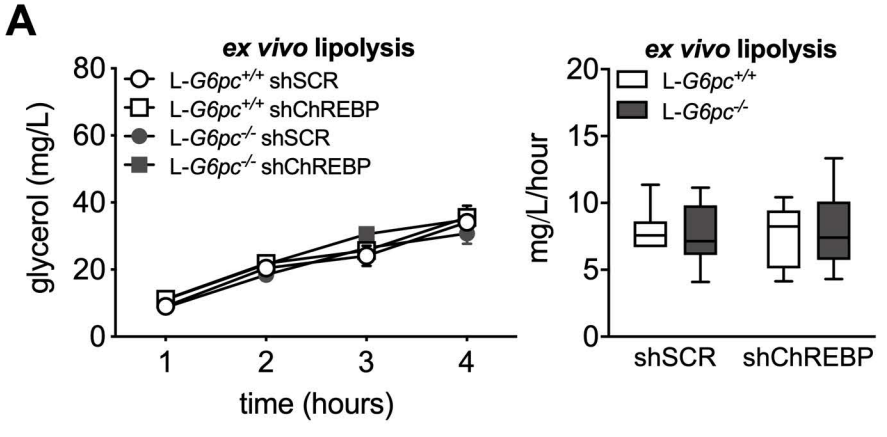
A
ex vivo lipolysis
L-G6pc+/+ shSCR
L-G6pc+/+ shChREBP
L-G6pc-/- shSCR
L-G6pc-/- shChREBP
glycerol (mg/L)
time (hours)
ex vivo lipolysis
L-G6pc+/+
L-G6pc-/-
mg/L/hour
shSCR
shChREBP

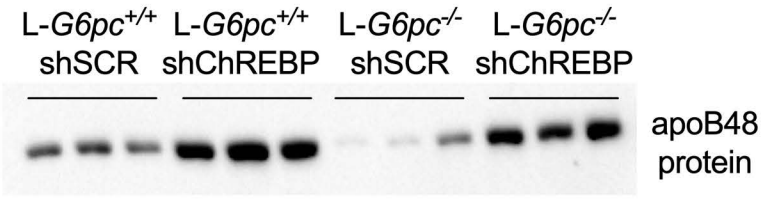
B
L-G6pc+/+ shSCR
L-G6pc+/+ shChREBP
L-G6pc-/- shSCR
L-G6pc-/- shChREBP
apoB48 protein

Figure S3

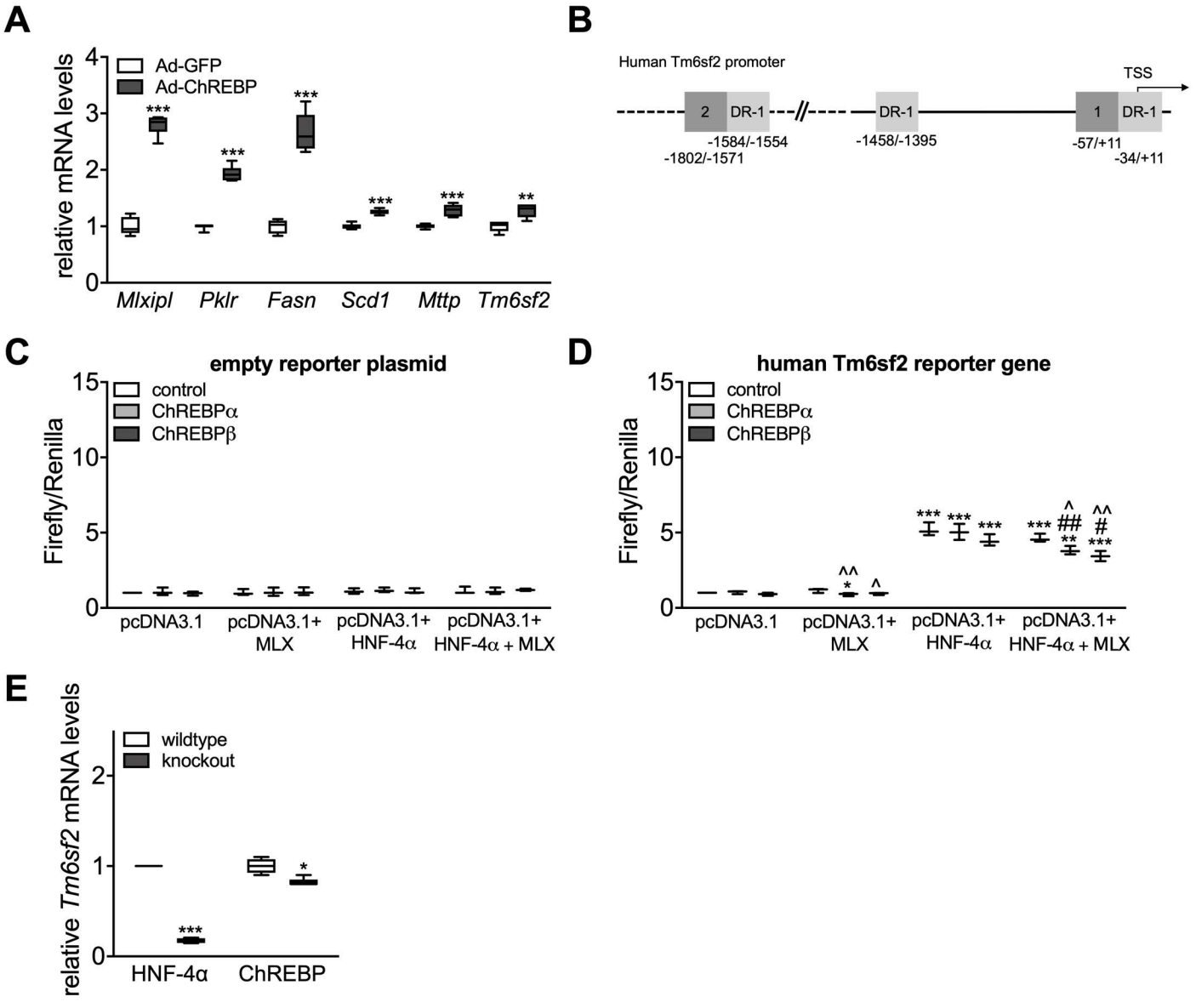
A
relative mRNA levels
Ad-GFP
Ad-ChREBP
Mlxipl
Pklr
Fasn
Scd1
Mttp
Tm6sf2
B
Human Tm6sf2 promoter
TSS
2
DR-1
DR-1
1
DR-1
-1584/-1554
-1802/-1571
-1458/-1395
-57/+11
-34/+11
C
empty reporter plasmid
Firefly/Renilla
control
ChREBPα
ChREBPβ
pcDNA3.1
pcDNA3.1+ MLX
pcDNA3.1+ HNF-4α
pcDNA3.1+ HNF-4α + MLX
D
human Tm6sf2 reporter gene
Firefly/Renilla
control
ChREBPα
ChREBPβ
pcDNA3.1
pcDNA3.1+ MLX
pcDNA3.1+ HNF-4α
pcDNA3.1+ HNF-4α + MLX
E
relative Tm6sf2 mRNA levels
wildtype
knockout
HNF-4α
ChREBP

Table S1. Taqman and SYBR Green qPCR primer and probe sequences used for qPCR and ChIP-qPCR

Gene	Method	Forward primer 5'- 3'	Reverse primer 5'- 3'	TaqMan probe 5'- 3'
Rplp0	Taqman qPCR	GCTTCATTGTGGGAGCAGACA	CATGGTGTTCTTGCCCATCAG	TCCAAGCAGATGCAGCAGATCCGC
Mlxipl isoform 1 (ChREBPα)	Taqman qPCR	CGACACTCACCCACCTCTTC	TTGTTCAGCCGGATCTTGTC	CCTGGCTTACAGTGGCAAGCTGGTCTCT
Mlxipl isoform 2 (ChREBPβ)	Taqman qPCR	TCTGCAGATCGCGTGGAG	CTTGTCCCGGCATAGCAAC	CTCAGTGGCAAGCTGGTCTCTCCCA
Apob	Taqman qPCR	GCCCATTGTGGACAAGTTGATC	CCAGGACTTGGAGGTCTTGGA	AAGCCAGGGCCTATCTCCGCATCC
Apobec	Taqman qPCR	TCGTCCGAACACCAGATGCT	GGTGTCGGCTCAGAAACTCTGT	CCTGGTTCCTGTCCTGGAGTCCCTG
Mttp	Taqman qPCR	CAAGCTCACGTACTCCACTGAAG	TCATCATCACCATCAGGATTCCT	ACCGCAAGACAGCGTGGGCTACA

Gapdh	SYBR qPCR	AAGATGGTGATGGGCTTCCCG	TGGCAAAGTGGAGATTGTTGCC
Rpl32	SYBR qPCR	TTAAGCGTAACTGGCGGAAACC	CAGTAAGATTTGTTGCACATCAGC
Tm6sf2	SYBR qPCR	CCC GGG AAA CAT CCT TGG TAA	GGG GTA TAG GAG GTT GGT GC
Tm6sf2 site 1	SYBR ChIP-qPCR	GAG CTT ATG GGC GGA GTCT	AGC TGG TCA CCA CCC TTT C
Tm6sf2 site 2	SYBR ChIP-qPCR	GGC GGA GTT ATA AGC TGG	GAG TGC CGC CCT ACT ATC AG
Tm6sf2 site 3	SYBR ChIP-qPCR	GGA GTA TGG GTA GGG CCT GT	GGA GAG GTC TGG GGA GGA T
Tm6sf2 site 4	SYBR ChIP-qPCR	AGT CCC AAT GCT CAC CTG TC	TTT GGA AGC CTC TTT TTC CTC